Journal of Organometallic Chemistry 693 (2008) 3603–3612

Contents lists available at ScienceDirect

Journal of Organometallic Chemistry

journal homepage: www.elsevier.com/locate/jorganchem

Synthesis, characterization and photovoltaic properties of a low-bandgap platinum(II) polyyne functionalized with a 3,4-ethylenedioxythiophene-benzothiadiazole hybrid spacer

Wai-Yeung Wong [a,*], Xingzhu Wang [a,b], Hai-Liang Zhang [b], Kai-Yin Cheung [c], Man-Kin Fung [c], Aleksandra B. Djurišić [c,*], Wai-Kin Chan [d]

[a] Department of Chemistry and Centre for Advanced Luminescence Materials, Hong Kong Baptist University, Waterloo Road, Hong Kong, PR China
[b] College of Chemistry and Key Laboratory of Low Dimensional Materials and Application Technology of Ministry of Education, Xiangtan University, Xiangtan 411105, Hunan Province, PR China
[c] Department of Physics, The University of Hong Kong, Pokfulam Road, Hong Kong, PR China
[d] Department of Chemistry, The University of Hong Kong, Pokfulam Road, Hong Kong, PR China

ARTICLE INFO

Article history:
Received 23 July 2008
Received in revised form 19 August 2008
Accepted 20 August 2008
Available online 26 August 2008

Keywords:
Polyynes
Metallopolymers
Photovoltaics
Ethylenedioxythiophene
Platinum

ABSTRACT

The synthesis, characterization and optical spectroscopy of a deep blue platinum(II) polyyne functionalized with the (3,4-ethylenedioxythiophene)-benzothiadiazole hybrid spacer (**P1**) and its dinuclear platinum molecular model complex (**M1**) are described. This metalated polymer **P1** exhibits good thermal stability and possesses a narrow bandgap of 1.76 eV. Optical spectroscopic measurements of these materials reveal a substantial donor–acceptor interaction along the rigid backbone of the organometallic polyynes through the interaction of metal center and the conjugated tricyclic ligand. Preliminary study shows that **P1:** methanofullerene acceptor blend can be used as an active layer of bulk-heterojunction polymer solar cells. Photoexcitation of this blend layer in some yet-to-be optimized cells results in a photo-induced electron transfer from the π-conjugated metallopolyyne electron donor to [6,6]-phenyl C_{61}-butyric acid methyl ester with a power conversion efficiency (PCE) close to 0.30% under air mass (AM1.5) simulated solar illumination. The power dependencies of the solar cell parameters (including the short-circuit current density, open-circuit voltage, fill-factor and PCE) were also studied.

1. Introduction

The discovery of the metal-like conductivity in oxidized poly(acetylene) and polyaromatic systems (e.g. polypyrrole, polythiophene or polyaniline) in the late seventies and early eighties [1–4] generated a considerable interest in functional π-conjugated systems. These systems have a potential use as organic semiconductors in a variety of applications, such as polymer light-emitting diodes [5–10], polymer solar cells (PSCs) [11–19], photodetectors [17], biosensors [20,21] and field-effect transistors [22,23]. Among these, much attention is currently paid to the development of novel conjugated materials [24–26] and polymers [27–34] as low-cost renewable energy resources to be exploited in photovoltaic technology [24–26].

At present, the optical bandgaps (E_g) of the substituted poly[*p*-phenylenevinylene] and the polythiophenes commonly used in the PSCs are typically 2.0–2.2 eV [12,35,36] and not optimized with respect to the solar spectrum (ca. 350–1500 nm) [19,37]. Organic solar cells are a major driving force for research in bandgap-engineering. However, polymers with $E_g > 2.0$ eV only absorb radiation in the UV and green part of the visible range. Therefore, chemists have been making efforts to synthesize new low-bandgap polymers (i.e. polymers with $E_g < 1.9$–2.0 eV) to harvest more photon energies at long wavelengths to increase the photocurrent.

With the emergence of the donor–acceptor (D–A) concept for bandgap reduction, a large series of purely organic polymers have been developed [38,39]. The basic idea is that conjugated systems with a regular alternation of electron-rich donor and electron-deficient acceptor groups will exhibit a broadening of the valence and conduction bands and thus bandgap reduction [38–42]. 2,1,3-Benzothiadiazole [38,43,44] and thiophene [45–48] derivatives have been widely used as π-conjugating spacers in push–pull chromophores designed for the production of low-bandgap conjugated polymers. Recently, photovoltaic devices based on a blend of [6,6]-phenyl C_{61}-butyric acid methyl ester (PCBM) and some of these low-bandgap conjugated organic polymers have been reported [49–52]. Apart from the thiophene ring, 3,4-ethylenedioxythiophene (EDOT) also occupies a prominent position as the functional component for conjugated polymers due, among other things, to the strong electron donor effect, the self-rigidification of the

* Corresponding authors. Tel.: +852 34117074; fax: +852 34117348.
E-mail addresses: rwywong@hkbu.edu.hk (W.-Y. Wong), dalek@hkucc.hku.hk (A.B. Djurišić).

0022-328X/$ - see front matter © 2008 Elsevier B.V. All rights reserved.
doi:10.1016/j.jorganchem.2008.08.025

structure by non-covalent intramolecular interactions as well as quinoidization of the conjugated system [53].

Although PSCs using organic polymers in a bulk-heterojunction (BHJ) architecture have been extensively studied, their metalated analogues remain under-explored [54,55]. Metallopolymers derived from platinum alkynyl structural units have shown promising results in this area recently [56–63]. While the field is still in its infancy, low-bandgap soluble π-conjugated organometallic polyynes have gained growing interest [56,60,61,63]. We have recently demonstrated efficient solar cells based on polyplatinyne:PCBM BHJ with high and tunable PCEs [56,60,61,63]. It is generally admitted that a conjugated system serving as donor in a BHJ solar cell should have a bandgap lower than 1.80 eV to achieve a better harvesting of the energy of solar photons. In fact, it has been shown that an optimal band gap value for a single junction cell is 1.5 eV, while the two absorbers in tandem cells should have gaps of 1.7 eV and 1.1 eV, respectively, to maximize efficiency [34].

Although this E_g value has been demonstrated for purely organic polymers, the problem is complicated by the lack of examples of narrow-gap organometallic polyynes. Most metal polyyne polymers characterized so far have large E_g (>2.0 eV) [64–67], which compare unfavorably with those of their organic counterparts. We report here the synthesis, characterization and photovoltaic properties of a new low-bandgap metallopolyyne **P1** with 4,7-bis[2′-(3,4-ethylenedioxythiophene)]-2,1,3-benzothiadiazole tricyclic chromophore as a versatile building block that use a donor–acceptor approach to achieve absorption in the almost red spectral region.

2. Results and discussion

2.1. Synthesis and chemical characterization

The synthesis and chemical structures of platinum-containing metallopolyyne (**P1**) and its well-defined model complex (**M1**) are shown in Scheme 1. 4,7-Dibromo-2,1,3-benzothiadiazole [44] was first coupled with a monosubstituted tributylstannyl derivative of EDOT utilizing the standard Stille chemistry [68] to give the tri-block 4,7-bis[2′-(3,4-ethylenedioxythiophene)]-2,1,3-benzothiadiazole system, which upon iodination with *N*-iodosuccinimide (NIS) can form **L1-I**. Conversion of the diiodo precursor to its corresponding trimethylsilyl-substituted congener **L1-2TMS** is accomplished via the typical organic synthetic routes for alkynylation of aromatic halides [69]. The platinum(II) compounds **P1** and **M1** were prepared by the Sonogashira dehydrohalogenative reactions between the diethynyl derivative (which should be prepared in situ under an inert atmosphere from the reaction of **L1-2TMS** with Bu_4NF in THF to avoid its rapid decomposition) and the platinum chloride or dichloride precursors in an amine solvent in the presence of CuI [56–67]. The phenyl end-capped complex **M1** represents a good molecular model compound for the elucidation of the spectroscopic and photophysical properties of **P1**. The polymer is purified by silica column chromatography and repeated precipitation. The structures of both materials were characterized using elemental analyses, mass spectrometry, IR and NMR spectroscopies. The NMR data are consistent with the proposed structure of **P1** and **M1**. The dichloromethane-soluble fraction of **P1** was isolated by Soxhlet extraction. The synthetic yield is not high for **P1** since a certain portion of the polymer formed under our experimental conditions was organic insoluble. As a consequence of the poorer solubility of **P1**, the molecular weight of the soluble fraction is believed to be relatively low (see Section 4). Th narrow polydispersity (PDI < 2) in molecular weights is consistent with the proposed linear structure from the condensation polymerization. Both **P1** and **M1** are air and thermally stable. Thermogravimetric analysis (TGA) traces (at a heating rate of 20 °C/min) showed the onset of the polymer decomposition at around 365 °C. Decomposition onset was defined by a 39 wt.-% loss for **P1**, corresponding to the removal of two PBu_3 ligands from **P1**. In differential scanning calorimetry (DSC) studies, no phase transition signals are detected during repeated heating/cooling DSC cycles for **P1** over the temperature range from 20 to 300 °C. This observation probably results from the stiffness of the polymer's chains.

Although 4,7-bis[2′-(3,4-ethylenedioxythiophene)]-2,1,3-benzothiadiazole has been reported before [44], its solid-state structure is not yet known. The X-ray crystal structure of this compound as well as that for **L1-2TMS** were determined and perspective views of the molecules are depicted in Fig. 1. From Fig. 1a, the molecule adopts a fully planar geometry with the dihedral angle between the S(1)- and S(2)-planes of only 3.1°. Furthermore, we note a short-contact hydrogen bonding interaction between H(9A) and O(2) [H(9A)···O(2) = 2.193 Å]. Close examination of the non-bonded distance between sulfur and nitrogen atoms of the adjacent cycles shows that the sulfur-nitrogen distance [S(1)···N(1) = 2.868 Å] is markedly smaller than the sum of the van der Waals radii of the individual atoms, thus demonstrating the existence of non-covalent intramolecular interactions which contribute to planarize the system [53]. For **L1-2TMS**, the two trimethylsilylacetylide groups are bonded to the central tricyclic ring which also reveals the involvement of non-bonded short contacts [S(1)···N(1) = 2.882, S(3)···N(2) = 2.848, H(16A)···O(3) = 2.201, H(17A)···O(2) = 2.218 Å] to ensure the planarity and rigid skeleton of the molecule. The S(2)-plane makes dihedral angles of 1.0° and 3.4° with the S(1)- and S(3)-planes, respectively. Thus, in addition to the electronic effects already observed in the tricyclic systems [53], EDOT introduces a self-rigidification effect which contributes to a further reduction of the bandgap.

2.2. Photophysical and electrochemical characterization

The photophysical properties of the polymer and model complex were measured in CH_2Cl_2 solutions at 293 K (Fig. 2 and Table 1). Fig. 2a shows the absorption spectra of **L1-2TMS**, **P1** and **M1** in CH_2Cl_2 (conc. $\sim 5 \times 10^5$ mol/dm^3), as well as **P1** in solid thin film. The spectra displayed two major absorption bands in each case. The lowest-energy absorption features are lowered significantly (by ca. 0.31 eV) when the metal is introduced in the polymer chain, i.e., on going from **L1-2TMS** to **P1**, which is expected for a donor–acceptor (D–A) π-conjugated framework [57,71,72]. The absorption properties of **M1** (λ_{max} = 385, 586 nm) are only slightly blue-shifted from those of **P1** (λ_{max} = 387, 590 nm). From the similar pattern of the absorption bands of ligand and polymer (Fig. 2a), we infer that the absorption is mainly due to the $\pi-\pi^*$ transition of the conjugated ligand from the highest occupied molecular orbital (HOMO) to the lowest unoccupied molecular orbital (LUMO), although the energy levels of the orbitals involved are perturbed by strong interactions with the metal center. Moreover, the absorption spectrum of the polymer in solid thin films is bathochromically shifted compared to that recorded in CH_2Cl_2 solution, presumably due to the interchain interactions in the film state. For many organic systems, it could be the case that aggregates consisting of many polymer chains are formed in the solid state, and the electronic communication of the π-systems via tight packing and a π–π stacking effect leads to the observed bathochromic shift. Alternatively, the occurrence of the red-shifted feature is a single-molecule effect, similarly to that for polythiophenes, in which planarization of the π-system is induced by aggregation [70]. The forced planarization then results in increased conjugation and thus leads to a lower E_g. The optical bandgap of 1.76 eV was estimated

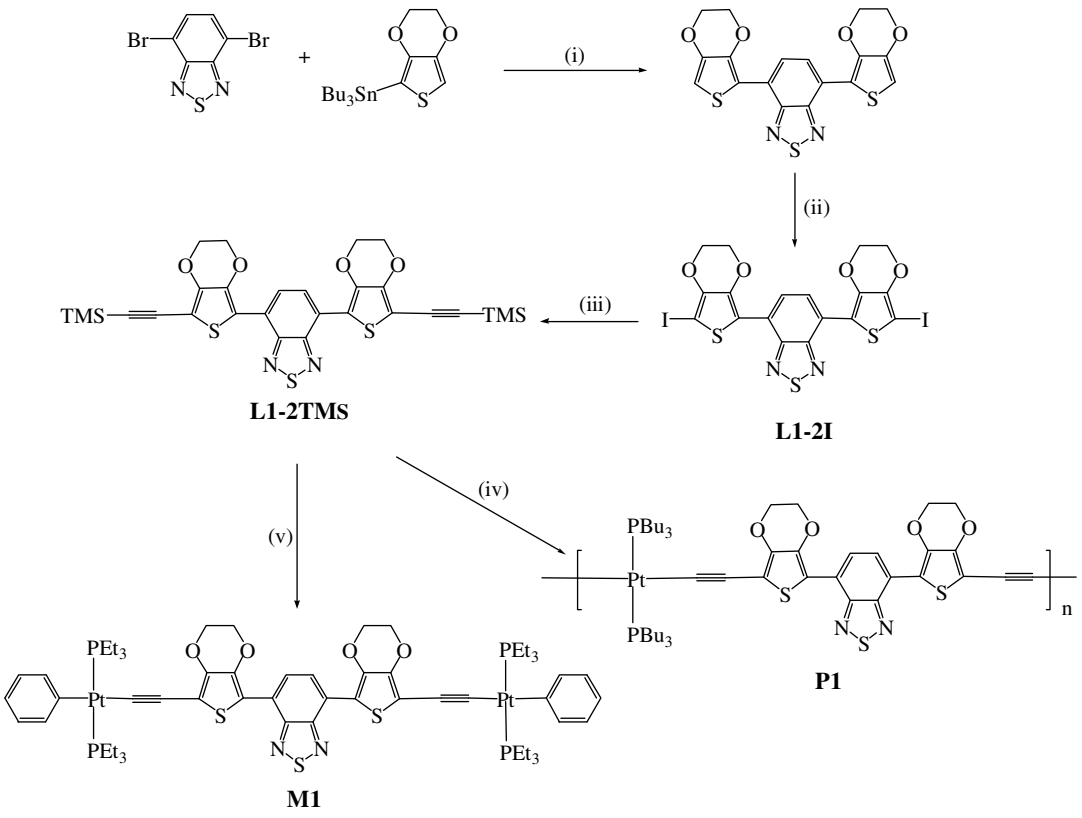

Scheme 1. Synthesis of metallopolymer **P1** and the model complex **M1**. Conditions and reagents: (i) $Pd(PPh_3)_4$, $PhCH_3$, reflux; (ii) $CHCl_3$/AcOH, NIS; (iii) $Me_3SiC{\equiv}CH$, $Pd(OAc)_2$, PPh_3, CuI, Et_3N; (iv) Bu_4NF, *trans*-$[Pt(PEt_3)_2PhCl]$, CuI, $^iPr_2NH/CH_2Cl_2$ and (v) Bu_4NF, *trans*-$[Pt(PBu_3)_2Cl_2]$, CuI, $^iPr_2NH/CH_2Cl_2$.

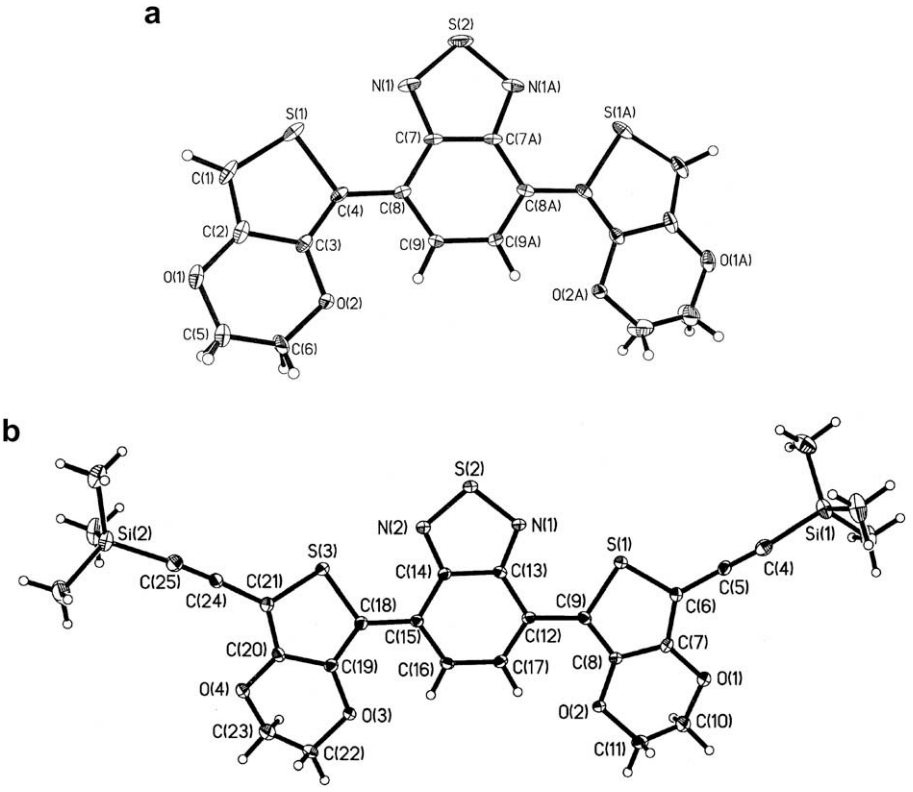

Fig. 1. X-ray crystal structures (with thermal ellipsoids drawn at 25% probability levels) of (a) 4,7-bis[2′-(3,4-ethylenedioxythiophene)]-2,1,3-benzothiadiazole. Selected bond lengths (Å) and angles [°]: S(1)–C(1), 1.704(5); S(1)–C(4), 1.741(4); C(4)–C(8), 1.445(6); S(2)–N(1), 1.608(4); C(7)–N(1), 1.354(5); N(1)–S(2)–N(1A), 101.1(3). (b) **L1-2TMS**. The labels on the methyl carbon atoms are omitted for clarity. Selected bond lengths (Å) and angles [°]: Si(1)–C(4), 1.858(5); C(4)–C(5), 1.158(5); S(1)–C(6), 1.729(4); S(1)–C(9), 1.743(4); C(9)–C(12), 1.469(5); S(2)–N(1), 1.620(3); S(2)–N(2), 1.610(3); C(15)–C(18), 1.465(5); S(3)–C(18), 1.742(4); S(3)–C(21), 1.734(4); Si(2)–C(25), 1.858(5); C(24)–C(25), 1.168(5); Si(1)–C(4)–C(5), 173.9(4); C(4)–C(5)–C(6), 177.4(5); N(1)–S(2)–N(2), 100.6(2); Si(2)–C(25)–C(24), 175.3(4); C(21)–C(24)–C(25), 176.3(4).

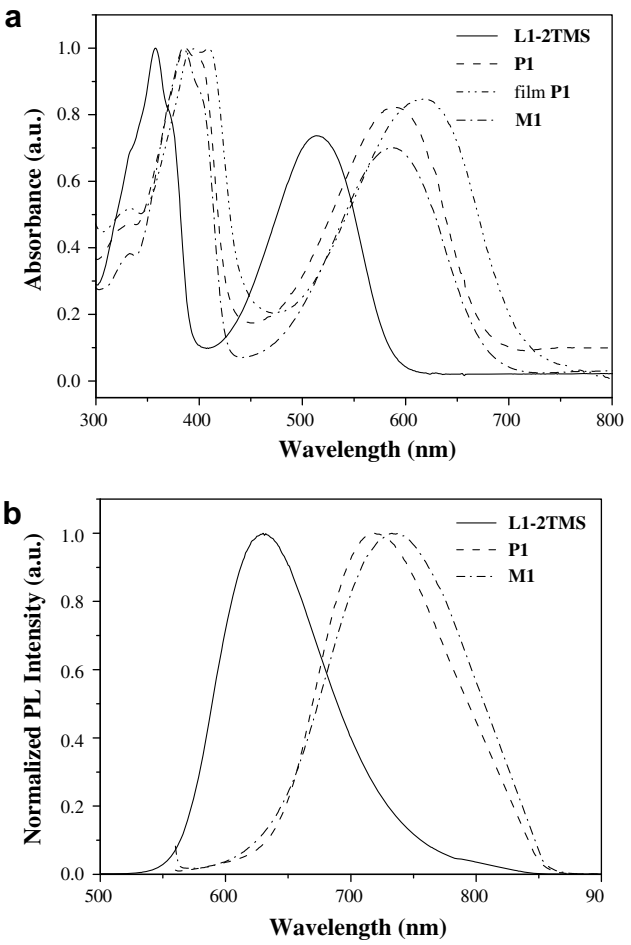

Fig. 2. (a) UV–Vis absorption and (b) PL spectra for **L1-2TMS**, **M1** and **P1**.

Table 1
Photophysical data of **L1-2TMS**, **M1** and **P1**

Samples	λ_{abs} in CH_2Cl_2 (nm)	λ_{em} in CH_2Cl_2 (nm)[b]	E_g (eV)[c]
L1-2TMS	357 (3.9), 513 (2.8)	630 (0.74, 10.5)	2.12
M1	332sh (1.7), 385 (4.4), 401sh (4.0), 586 (3.1)	732 (0.026, 2.27)	1.84
P1	332sh, 387, 398sh, 590 (333sh, 368sh, 389, 407sh, 619)[a]	720 (0.021, 2.51)	1.83 (1.76)[d]

[a] λ_{abs} values obtained from thin film.
[b] Emission quantum yields (Φ) and lifetimes (τ) in ns are shown in parentheses (Φ, τ). λ_{ex} = 500 nm.
[c] Optical bandgaps obtained from absorption spectra in CH_2Cl_2.
[d] Optical bandgap from the solid-state thin film spectrum.

from the onset of solid-state absorption spectrum. There is only a small difference in E_g between **P1** and **M1**. To date, the value of 1.76 eV is one of the lowest among the reported polyplatinynes and clearly represents a significant step forward in the development of low-bandgap metallopolyyne polymers [64–67]. The significant D–π–A structural motif constitutes a major tool for the modulation of the electronic properties of extended systems and has an immediate effect on the resulting optical properties. Table 2 compares the solid-state colors, E_g and thermal stability data of **P1** with some related platinum(II) polyynes in the literature in terms of their π-conjugating ability in which the addition of suitable acceptor groups tends to reduce E_g accompanied by a shift of λ_{max} to the red. Due to the presence of a more extended π-electron delocalized system throughout the chain and the creation of an alternate D–A chromophore based on an electron-accepting benzothiadiazole group in combination with the electron-donating EDOT rings, the E_g value of **P1** is significantly reduced by ca. 0.79 eV relative to the purely electron-rich bithienyl (2.55 eV) congener [59]. A reduction of the bandgap by 0.44 eV is achieved in **P1** upon adding one EDOT ring on each side of benzothiadiazole, which results in onset of optical absorption at 590 nm. An increase of the donor strength in **P1** with the electron-releasing ethylenedioxy bridge leads to a bathochromic shift of λ_{max} accompanied by a decrease in E_g relative to that with a 4,7-di-2′-thienyl-2,1,3-benzothiadiazole spacer. Comparison of the electronic absorption spectrum of **P1** to those of terthienyl counterpart also reveals a considerable red shift of the absorption maximum indicative of the reduction of the HOMO-LUMO gap. The triblock heteroaromatic spacer in **P1** with a functional median group inserted between two lateral EDOT groups already has a strong D–A interaction which can be enhanced by the extensive π-delocalization in the conjugated polymer backbone containing the electron-rich platinum (Fig. 3). This reflects an important role of strong D–A interaction in **P1**, which is created by a regular alternation of D- and A-like moieties, possibly separated by neutral parts. If the electron donor and acceptor regions are extended through the Pt center and alkynyl units we get a system analogous to the inorganic n-i-p-i superlattice quantum well structure that exhibit a much lower E_g [71,72].

The photoluminescence (PL) spectra of **P1** and **M1** are depicted in Fig. 2b. They displayed one strong structureless peak in the near-infrared region at 720 and 732 nm, respectively. Compared to the Pt polyyne with bis(thienyl)-benzothiadiazole which fluoresces at 680 nm in CH_2Cl_2, we note a clear red shift in the emission wavelength for **P1** ($\Delta\lambda$ = 40 nm). The measured emission lifetime in the nanosecond range for **P1** and **M1** (2.51 and 2.27 ns, respectively) suggests a radiative decay from the singlet excited state (i.e. fluorescence). There is no emission from the long-lived triplet excited state over the measured spectral window between 1.2 and 3.1 eV for **P1** and **M1**. This can be explained in terms of the energy gap law for non-radiative decay for conjugated Pt polyynes and their molecular diynes, whereby the non-radiative decay rate increases exponentially with decreasing triplet–singlet energy gap according to the expression $(k_{nr})_P \propto \exp(-A\Delta E_{S-T})$, where ΔE_{S-T} is the energy gap for the T_1-S_0 transition and A is a term controlled by the molecular parameters and vibrational modes [74]. This phenomenon also involves the bandgap/phosphorescence decay rate trade-off commonly observed in such systems. Hence, a high-E_g polymer will favor phosphorescence whereas a low E_g value will be detrimental for the triplet emission. The fully extended heteroaryl rings in the ligand chromophore greatly reduces the influence of heavy Pt ion which is mainly responsible for the intersystem crossing and the phosphorescence. Hence, it is not the triplet state but a

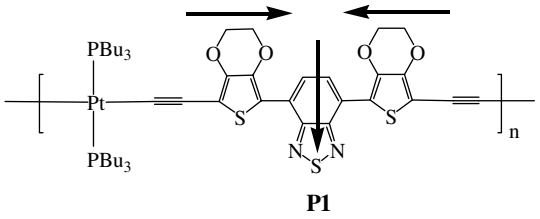

P1

Fig. 3. The expected direction of electron transfer after excitation in metallopolymer **P1**.

Table 2
Structural effects on the optical and thermal stability data of various low-bandgap platinum(II)-based metallopolyynes with different central spacer Ar

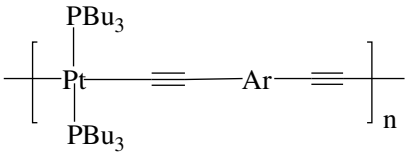

Ar	Color	Peak λ_{max} in solid film (nm)	E_g (eV)	T_{dec} (°C)	Ref.
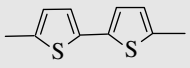	Yellow	446	2.55	278	[59]
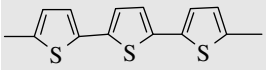	Orange-yellow	484	2.40	290	[59]
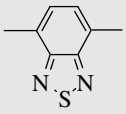	Orange-red	528	2.20	Not reported	[73]
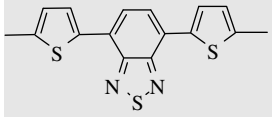	Purple	548	1.85	284	[60]
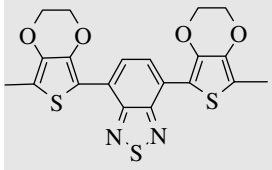	Deep blue	616	1.76	365	This work

ligand-based $\pi-\pi^*$ excited state that contributes to the photoinduced charge separation in the energy conversion for **P1** without the participation of the triplet state [57].

The HOMO and LUMO energy levels of **P1** were calculated using the onset oxidation and reduction potentials as determined from cyclic voltammetric method. The experiments were performed by casting the polymer films on the glassy-carbon working electrode with a Ag/AgCl wire as the reference electrode, at a scan rate of 50 mV s^{-1}. The solvent in all measurements was deoxygenated MeCN, and the supporting electrolyte was 0.1 M [$^nBu_4N$][BF_4]. From the onset values of oxidation ($E_{onset,ox}$) and reduction ($E_{onset,red}$), the HOMO and LUMO levels of **P1** were calculated according to the following equations $E_{HOMO} = -(E_{onset,ox} + 4.72)$ eV and $E_{LUMO} = -(E_{onset,red} + 4.72)$ eV (where the unit of potential is *V* vs. Ag/AgCl) [75]. **P1** shows a quasi-reversible oxidation wave with the $E_{onset,ox}$ at 0.62 V, giving rise to a HOMO level of −5.34 eV. Oxidation arises from the π-conjugated heteroaromatic segment of **P1**. The elevated HOMO level of **P1** relative to the one with dithienyl-benzothiadiazole unit (−5.37 eV) corroborates with the stronger donor property of the EDOT groups in the former case, which is also consistent with the absorption data shown above. The LUMO level of **P1** was then estimated to be −3.74 eV for measurements obtained from a polymer thin film.

2.3. Polymer photovoltaic behavior

To examine if the low-energy absorption band of **P1** contributes to the photovoltaic energy conversion in PSCs, BHJ solar cells were fabricated by using **P1** as an electron donor and PCBM as an electron acceptor (Table 3). The hole collection electrode consisted of indium tin oxide (ITO) with a spin-coated poly(3,4-ethylenedioxythiophene):poly(styrene sulfonate) (PEDOT:PSS), while Al served

Table 3
Solar cell performance of best devices with **P1**

PSC	V_{oc} (V)	J_{sc} (mA cm^{-2})	FF	Max. PCE (%)	Max. EQE (%)[c]
P1:PCBM (1:5)[a]	0.55 (0.54)	1.68 (1.68)	0.32 (0.31)	0.29 (0.28)	8.5 (567)
P1:PCBM (1:5)[b]	0.53 (0.53)	1.93 (1.83)	0.28 (0.28)	0.28 (0.27)	10.2 (567)

The numbers in parentheses denote average from 6 devices.
[a] Obtained from toluene.
[b] Obtained from chlorobenzene.
[c] For EQE maxima, the numbers in brackets denote the wavelength in nm at which maximum occurs.

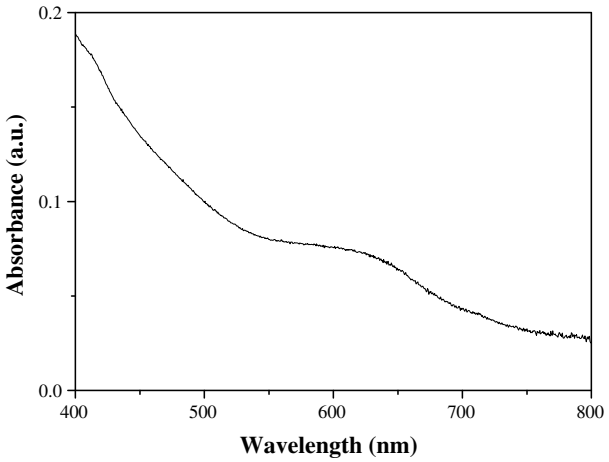

Fig. 4. The absorption spectrum of the **P1**:PCBM (1:5) active blend layer.

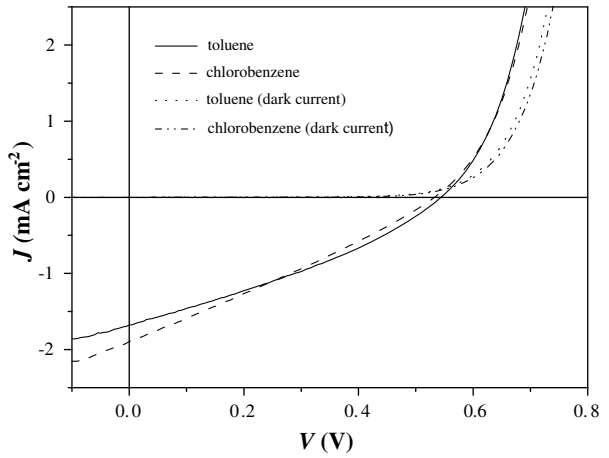

Fig. 5. *J–V* curves of the polymer solar cells with **P1**:PCBM active layers (at the blend ratio of 1:5 w/w) in the dark and under simulated AM1.5 solar irradiation.

as the electron collecting electrode. The absorption spectrum of **P1** blended with PCBM (1:5 by weight) is shown in Fig. 4, which shows a broad band peaking at around 600 nm. The higher energy peak in the blend film is less pronounced because of the dramatically enhanced absorption in the UV region due to PCBM. Fig. 5 displays the current density–voltage (*J–V*) characteristics of the PSCs recorded under air mass (AM 1.5) simulated solar illumination and the corresponding dark current curves. The BHJ devices (1:5 blend ratio) prepared from toluene solution exhibited an open-circuit voltage V_{OC} of 0.55 V, a short-circuit current density J_{SC} of 1.68 mA/cm^2, and a fill factor (FF) of 0.32, corresponding to a PCE of ~0.29%. Similar values were obtained from the chlorobenzene solvent. These values are comparable to those for some low-band-gap near-infrared-absorbing organic polymer diodes reported in the literature [51,76]. It should be noted that in spite of low band-gap, the obtained power conversion efficiency of this polymer is not as high as that obtained for other low bandgap metal-containing polymers [60,61]. There are several possible reasons for that, such as lower absorption, lower molecular-weight as well as solubility yielding unfavorable phase separation and film quality and morphology. The J_{SC} and FF values are relatively low, which in addition to factors mentioned above can also be affected by processing and measurement in ambient atmosphere, which can result in the presence of traps. In addition, J_{SC} and FF would be affected by the charge collection efficiency, which is in turn affected by the blend film morphology. Comprehensive study of phase separation in the blend, film morphology and charge transport is necessary to further improve FF and overall device performance.

The external quantum efficiency (EQE) for the solar cells has been measured, as shown in Fig. 6. All EQE curves of the polymer photodiodes show onset near 750 nm, and there is a photoinduced charge transfer from the polymer to PCBM. The EQE photoaction spectrum shows a major peak at around 567 nm that corresponds to the absorption spectral profile of **P1**. The similarity of the absorption spectrum and EQE response demonstrates that the excitons produced by absorption in the polymer are dissociated into charge carriers at the contact between **P1** and PCBM in the active layer, and are subsequently collected at the electrodes. The broad EQE curves for **P1** cover the visible-light region from 400 up to ~800 nm with maxima values of 8.5–10.2%. In addition to other prerequisites of the donor materials such as their electronic properties and absorption ability, they must combine solution processability and appropriate compatibility with PCBM to provide a composite material with optimal nanoscale morphology. Nevertheless, these devices are still not fully optimized and similar materials of different molecular weight ranges are anticipated to show better results. Further studies are currently underway to obtain devices of higher performance.

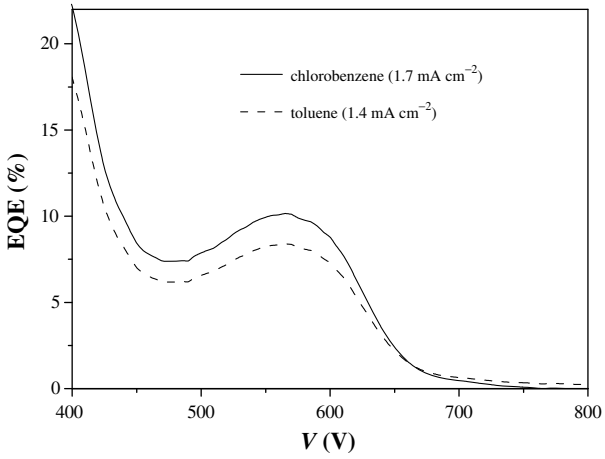

Fig. 6. EQE wavelength dependencies of solar cells with **P1**:PCBM (1:5) active layers.

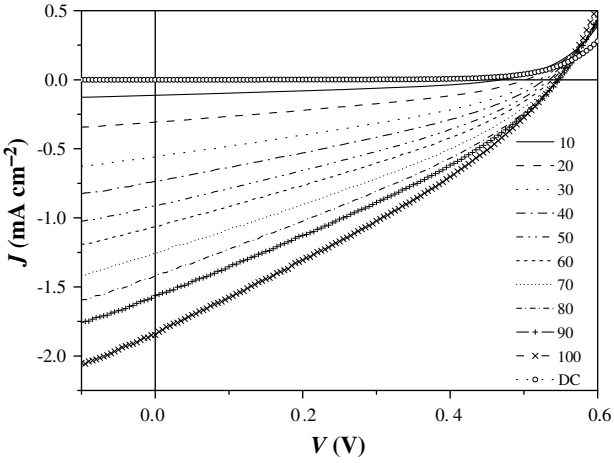

Fig. 7. *J–V* curves of the **P1**:PCBM (1:5) device for different illumination power (in units of mW cm^{-2}). The dark current (DC) curve is also included.

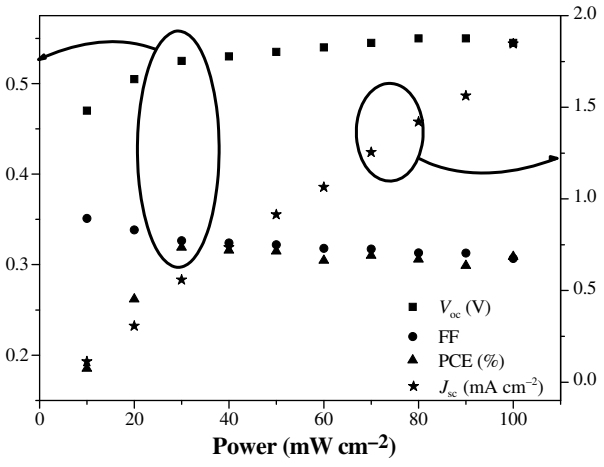

Fig. 8. Power dependencies of open-circuit voltage (V_{OC}), short-circuit current density (J_{SC}), fill factor (FF) and power conversion efficiency (PCE) for the **P1**:PCBM (1:5) cells.

To study the performance of PSCs, it is important to understand which mechanisms control the $J-V$ characteristics of a given device and the fate of the photogenerated electrons and holes. So, the influence of light intensity on the solar cell parameters is very informative for analyzing internal recombination losses [77]. The $J-V$ curves for **P1** under different excitation powers and the power dependence of the solar cell parameters are shown in Figs. 7 and 8, respectively. The J_{SC} exhibits a linear dependence on the optical power, while V_{oc} shows some increase and then saturates at higher intensity, as expected [78]. The almost linear photocurrent dependence on the light intensity for voltage approaching V_{OC} does not give a slope of ~¾, which indicates the absence of space-charge-limited device performance and that the charge-carrier losses in the absorber bulk are dominated by monomolecular recombination under short-circuit conditions. The PCE only decreases slightly with the illumination intensity, reaching a peak of 0.32% at 30 mW cm^{-2}. The FF shows a maximum of 0.35 at a low power level of 10 mW cm^{-2} but drops gradually at higher light intensities, in agreement with previously reported power dependence of FF in a BHJ cell [79]. In another trial on another polymer sample of comparable molecular weights, we even witnessed a PCE = 0.42% at 20 mW cm^{-2} (see Figs. S1 and S2 in Supporting Information) and similar trends in the device performance parameters were observed.

3. Conclusion

In summary, a metalated push–pull conjugated polymer using 3,4-ethylenedioxythiophene as the donor group and 2,1,3-benzothiadiazole as the acceptor block was prepared and characterized. Optical spectroscopy suggests a very narrow bandgap system for this polymer. Preliminary results on unoptimized BHJ solar cells indicate a PCE of 0.30% under solar-light illumination in AM 1.5 conditions. The present work emphasizes good opportunities offered by the EDOT building block for the design and synthesis of new classes of functional π-conjugated metallopolymers for advanced electronic and photonic applications. To further improve the solubility and solution-processability of this type of highly conjugated polyaromatic structure we should aim at a parent organic precursor in which EDOT is substituted by a long alkoxy chain grafted at the ethylenedioxy bridge. Also, device optimization requires further studies of the blend morphology and charge transport in the blends with different compositions. It is expected that optimization at all levels of device construction and composition will result in further improvements in the efficiency. The dependence of solar cell performance on molecular weight should not be overlooked, which can cause significant changes in the blend morphology, and polymers of higher molecular weights should benefit to the overall performance.

4. Experimental

4.1. General information

Solvents were carefully dried and distilled from appropriate drying agents prior to use. Commercially available reagents were used without further purification unless otherwise stated. *trans*-[$PtCl_2(PBu_3)_2$] [80] and *trans*-[$PtPh(Cl)(PEt_3)_2$] [81] were prepared as described in the literature. All reagents for chemical syntheses were purchased from Aldrich or Acros Organics. PCBM was purchased from American Dyes. PEDOT:PSS (Baytron VPAI 4083) was purchased from H.C. Starck. Reactions and manipulations were carried out under an atmosphere of prepurified nitrogen using Schlenk techniques. All reactions were monitored by thin-layer chromatography (TLC) on silica with Merck pre-coated glass plates. Flash column chromatography was carried out using silica gel from Merck (230–400 mesh).

4.2. Physical measurements

Infrared spectra were measured as CH_2Cl_2 solutions using a Perkin–Elmer Paragon 1000 PC FTIR spectrometer. Fast atom bombardment (FAB) mass spectra were recorded on a Finnigan MAT SSQ710 system. NMR spectra were measured in $CDCl_3$ on a Varian Inova 400 MHz FT-NMR spectrometer and chemical shifts are quoted relative to tetramethylsilane for ^1H and ^{13}C nuclei and H_3PO_4 for ^{31}P nucleus. UV–Vis spectra were obtained on an HP-8453 diode array spectrophotometer. The emission spectra of the polymers were measured on a Photon Technology International (PTI) Fluorescence QuantaMaster Series QM1 spectrophotometer. The emission quantum yields (Φ) were determined in CH_2Cl_2 solutions at 293 K against the Rhodamine B in EtOH standard [82]. The CV measurements were carried out at a scan rate of 50 mV/s using a eDAQ EA161 potentiostat electrochemical interface equipped with a thin film coated ITO covered glass working electrode, a platinum counter electrode and a Ag/AgCl (in 3 M KCl) reference electrode. The solvent in all measurements was deoxygenated MeCN, and the Supporting electrolyte was 0.1 M [$^nBu_4N$][BF_4]. Thin polymer films were deposited on the working electrode by dip coating in chlorobenzene solution (6 mg/cm^3). The onset oxidation and reduction potentials were used to determine the HOMO and LUMO energy levels using the equations $E_{HOMO} = [-(E_{onset,ox\ (vs.\ Ag/AgCl)} - E_{onset\ (N.H.E.\ vs.\ Ag/AgCl)})] - 4.50$ eV and $E_{LUMO} = [-(E_{onset,red\ (vs.\ Ag/AgCl)} - E_{onset\ (N.H.E.\ vs.\ Ag/AgCl)})] - 4.50$ eV, where the potentials for N.H.E. vs. vacuum and N.H.E. vs. Ag/AgCl are 4.50 and −0.22 V, respectively [75]. The molecular weights of the polymer were determined by GPC (HP 1050 series HPLC with visible wavelength and fluorescent detectors) using polystyrene standards and THF as eluent. Thermal analyses were performed with the Perkin–Elmer Pyris Diamond DSC and the Perkin–Elmer TGA6 thermal analyzers.

4.3. Preparation of compounds

4.3.1. Preparation of 2-tributylstannyl-3,4-ethylenedioxythiophene

To a solution of 3,4-ethylenedioxythiophene (2.30 g, 160 mmol) and *N*,*N*,*N*′,*N*′-tetramethylethylenediamine (TMEDA) (2.10 g, 185 mmol) in anhydrous diethyl ether (60 mL), a solution of *n*-butyllithium (10.0 mL, 160 mmol, 1.6 M in hexane) was slowly added using a syringe under an argon atmosphere at room temper-

ature. The mixture was stirred at room temperature for 10 min, and then refluxed for 30 min. A pink, milk-like mixture was formed. The mixture was cooled to −78 °C, and tributyltin chloride (5.18 g, 160 mmol) was added slowly to it over 1.5 h. The reaction mixture was warmed up to room temperature and stirred for 3 h. After it was quenched with saturated sodium chloride solution (50 mL), its organic layer was extracted with diethyl ether (3 × 50 mL), dried over $MgSO_4$, and filtered. Triethylamine (10 mL) was added to the filtrate, and the solvents were evaporated. The residue was purified using column chromatography with hexane on a pre-treated silica gel (silica gel was washed with neat triethylamine, and then with hexane). The solvent was removed under vacuum and the residue was further purified through vacuum distillation to produce a colorless liquid (yield: 75%); ^{1}H NMR ($CDCl_3$, δ): 6.59 (s, 1H, thienyl), 4.17 (m, 4H, ethylene), 1.58 (m, 6H, $SnCH_2$), 1.35 (m, 6H, CH_2), 1.11 (m, 6H, CH_2), 0.91 ppm (t, J = 7.2 Hz, 9H, CH_3).

4.3.2. Preparation of 4,7-bis[2′-(3,4-ethylenedioxythiophene)]-2,1,3-benzothiadiazole

$Pd(PPh_3)_4$ (20.0 mg) was added to a solution of 4,7-dibromo-2,1,3-benzothiadiazole (1.47 g, 5.00 mmol) and 2-tributylstannyl-3,4-ethylenedioxythiophene (5.40 g, 12.5 mmol) in toluene (50 mL). The mixture was refluxed in a nitrogen atmosphere for 12 h, and the mixture was then cooled to room temperature, after which the solvent was removed under reduced pressure. The product was purified by column chromatography eluting with hexane/CH_2Cl_2 (1:2, v/v) to give a red solid in 65% yield (2.70 g). ^{1}H NMR ($CDCl_3$, δ): 8.39 (s, 2H, benzo), 6.56 (s, 2H, thienyl), 4.41–4.39 (m, 4H, ethylene), 4.32–4.30 ppm (m, 4H, ethylene). ^{13}C NMR ($CDCl_3$, δ): 152.36, 141.67, 140.27, 126.65, 123.7, 113.74, 101.98 (Ar), 65.01, 64.37 ppm (CH_2). FAB-MS: m/z 416 (M^+). Anal. Calc. for $C_{18}H_{12}N_2O_4S_3$: C, 51.91; H, 2.90; N, 6.73. Found: C, 51.78; H, 3.02; N, 6.83%.

4.3.3. Preparation of L1-2I

4,7-Bis[2′-(3,4-ethylenedioxythiophene)]-2,1,3-benzothiadiazole (417 mg, 1.0 mmol) was dissolved in a mixture of chloroform (30 mL) and acetic acid (30 mL) under a nitrogen atmosphere, and *N*-iodosuccinimide (490 mg, 2.20 mmol) was immediately added. After the reaction mixture had been stirred at room temperature for 6 h, it was then poured into cold water and the mixture was extracted with chloroform. The organic layer was washed twice with water and dried over $MgSO_4$. The solution was then concentrated under vacuum and methanol was added. The precipitate formed was filtered off, washed with methanol and dried in an oven to give the crude product, which was recrystallized from a mixture of CH_2Cl_2 and hexane (1:3, v/v) to afford a dark red solid in 87% yield (582 mg). ^{1}H NMR ($CDCl_3$, δ): 8.35 (s, 2H, benzo), 4.39 ppm (m, 8 H, ethylene). FAB-MS: m/z 668 (M^+). Anal. Calc. for $C_{18}H_{10}N_2I_2O_4S_3$: C, 32.35; H, 1.51; N, 4.19. Found: C, 32.45; H, 1.56; N, 4.34%.

4.3.4. Preparation of L1-2TMS

To an ice-cooled mixture of **L1-2I** (669 mg, 1.00 mmol) in freshly distilled triethylamine (20 mL) and CH_2Cl_2 (20 mL) was added CuI (20.0 mg) and $Pd(OAc)_2$ (60.0 mg). After the solution was stirred for 30 min, trimethylsilylacetylene (0.15 mL, 1.00 mmol) was then added and the suspension was stirred for 30 min in an ice-bath before being warmed to room temperature. After reacting for 30 min at room temperature, the mixture was heated to 50 °C for 24 h. The solution was then allowed to cool to room temperature and the solvent mixture was evaporated *in vacuo*. The crude product was purified by column chromatography on silica gel with a solvent combination of hexane/CH_2Cl_2 (2:5, v/v) as eluent to provide **L1-2TMS** as a dark red solid (430 mg, 71%). IR (KBr): ν(C≡C) 2135 cm^{-1}. ^{1}H NMR ($CDCl_3$, δ): 8.41 (s, 2H, benzo), 4.39 (m, 8H, ethylene), 0.27 ppm (s, 18H, TMS). ^{13}C NMR ($CDCl_3$, δ): 152.09, 144.26, 139.40, 127.00, 123.40, 114.92, 104.15, 100.95, 94.95 (Ar), 64.76, 64.72 (CH_2), 0.00 ppm (TMS). FAB-MS: m/z 608 (M^+). Anal. Calc. for $C_{28}H_{28}N_2O_4S_3Si_2$: C, 55.23; H, 4.64; N, 4.60. Found: C, 55.38; H, 4.55; N, 4.80%.

4.3.5. Synthesis of platinum metallopolyyne *P1*

Polymerization was carried out by mixing **L1-2TMS** (25 mg, 0.04 mmol), *trans*-$[Pt(PBu_3)_2Cl_2]$ (27 mg, 0.04 mmol) and CuI (2.0 mg) in ^{i}Pr$_2$NH/CH_2Cl_2 (40 mL, 1:1, v/v). Bu_4NF (0.08 mL of a 1 M solution in THF) was subsequently added and the solution quickly turned deep blue. After stirring at room temperature for 20 h under nitrogen, the solution mixture was evaporated to dryness. The residue was redissolved in CH_2Cl_2 and filtered through a short silica column using the same eluent to remove the ionic impurities and catalyst residues. After removal of the solvent, the crude product was purified twice by precipitation in CH_2Cl_2 from MeOH. Subsequent washing with hexane and drying *in vacuo* gave a deep blue solid of **P1** (23 mg, 53%). IR (KBr): ν(C≡C) 2099 cm^{-1}. NMR ($CDCl_3$, δ): 8.39 (s, 2H, benzo), 4.35 (m, 4H, ethylene), 4.28 (m, 4H, ethylene), 2.22−2.07 (m, 12 , CH_2), 1.59−1.46 (m, 24H, CH_2), 0.99−0.94 ppm (m, 18H, CH_3); ^{31}P NMR ($CDCl_3$, δ): 3.40 ppm ($^1J_{P-Pt}$ = 2390 Hz). GPC (THF): M_w = 5400, M_n = 8800, M_w/M_n = 1.63. Anal. Calc. for $(C_{46}H_{64}N_2O_4P_2PtS_3)_n$: C, 52.01; H, 6.07; N, 2.64. Found: C, 52.43; H, 6.18; N, 2.98%.

4.3.6. Synthesis of platinum model complex *M*

To a stirred mixture of **L1-2TMS** (13.0 mg, 0.02 mmol) in ^{i}Pr$_2$NH (10 mL) and CH_2Cl_2 (10 mL) was added *trans*-$[Pt(PEt_3)_2PhCl]$ (23 mg, 0.04 mmol) and CuI (1.0 mg). Bu_4NF (0.04 mL of a 1 M solution in THF) was added. The solution was stirred at room temperature under nitrogen over a period of 24 h, after which all volatile components were removed under vacuum. The crude product was taken up in CH_2Cl_2 and purified on preparative silica TLC plates with hexane/CH_2Cl_2 (2:5, v/v) as eluent. The product **M** was obtained as a deep blue solid (18 mg, 62%). IR (KBr): ν(C≡C) 2080 cm^{-1}. ^{1}H NMR ($CDCl_3$, δ): 8.34 (s, 2H, benzo), 7.32 (d, J = 7.2 Hz, 4H, H_{ortho} of Ph), 6.97 (t, J = 7.4 Hz, 2H, H_{meta} of Ph), 6.80 (t, J = 7.2 Hz, 4H, H_{para} of Ph), 4.37–4.35 (m, 4H, ethylene), 4.31–4.30 (m, 4H, ethylene), 1.82–1.75 (m, 24H, CH_2), 1.14−1.06 ppm (m, 36H, CH_3). ^{13}C NMR ($CDCl_3$, δ): 156.32, 152.49, 141.23, 140.02, 139.20, 127.26, 127.02, 126.05, 123.10, 121.19, 109.61, 108.19, 99.40 (Ar + C≡C), 64.83, 64.29 (ethylene), 15.09, 8.10 ppm (Et); ^{31}P NMR ($CDCl_3$, δ): 9.85 ppm ($^1J_{P-Pt}$ = 2628 Hz). FAB-MS: m/z: 1478 (M^+). Anal. Calc. for $C_{58}H_{80}N_2O_4P_2Pt_2S_3$: C, 47.09; H, 5.45; N, 1.89. Found: C, 46.82; H, 5.23; N, 2.02%.

4.4. Solar cell fabrication and characterization

The device structure was ITO/poly(3,4-ethylenedioxythiophene):poly(styrene sulfonate) (PEDOT:PSS)/polymer:PCBM blend/Al. ITO glass substrates (10 Ω per square) were cleaned by sonication in toluene, acetone, ethanol and deionized water, dried in an oven, and then cleaned with UV ozone for 300 s. As-received PEDOT:PSS solution was passed through the 0.45 μm filter and spin-coated on patterned ITO substrates at 5000 r.p.m. for 3 min, followed by baking in N_2 at 150 °C for 15 min. The metallopolyyne:PCBM active layer (1:5 w/w) was prepared by spin-coating each of the chlorobenzene or toluene solutions at 1000 r.p.m. for 2 min. The substrates were dried at room temperature in low vacuum (vacuum oven) for 1 h, and then stored in high vacuum (10^{-5}−10^{-6} Torr) overnight. Al electrode (100 nm) was evaporated through a shadow mask to define the active area of the devices (2 mm circle). All the fabrication procedures (except drying, PED-

Table 4
Crystal data for 4,7-bis[2′-(3,4-ethylenedioxythiophene)]-2,1,3-benzothiadiazole (**EDOT-BTD-EDOT**) and **L1-2TMS**

	EDOT-BTD-EDOT	L1-2TMS
Formula	$C_{18}H_{12}N_2O_4S_3$	$C_{28}H_{28}N_2O_4S_3Si_2$
M_r	416.48	608.88
Crystal size (mm)	0.30 × 0.28 × 0.12	0.30 × 0.24 × 0.15
Crystal system	Orthorhombic	Monoclinic
Space group	*Pbcn*	*C*2/*c*
a (Å)	4.3945(6)	41.462(5)
b (Å)	15.655(2)	8.258(1)
c (Å)	23.950(3)	17.814(2)
α (°)	90	90
β (°)	90	105.450(2)
γ (°)	90	90
V (Å^3)	1647.7(4)	5878(1)
Z	4	8
D_{calc} (mg m^{-3})	1.679	1.376
μ (mm^{-1})	0.481	0.371
F(000)	856	2544
2θ Range (°)	2.60–25.00	2.32–25.00
Number of reflections collected	6693	13502
Number of unique reflections	1400	5142
R_{int}	0.0295	0.0458
Number of reflections with $I > 2.0\sigma(I)$	1253	3428
Number of parameters	123	352
R_1, wR_2 [$I > 2.0\sigma(I)$][a]	0.0649, 0.1383	0.0541, 0.1372
R_1, wR_2 (all data)[a]	0.0713, 0.1425	0.0901, 0.1538
Goodness-of-fit on F^2[b]	1.069	1.023

[a] $R_1 = \sum ||F_o|| - ||F_c|| / \sum ||F_o|| \cdot wR_2 = \left\{ \sum [w(F_o^2 - F_c^2)^2 / \sum [w(F_o^2)^2] \right\}^{1/2}$.
[b] GoF $= [(\sum w||F_o|| - ||F_c||)^2 / (N_{obs} - N_{param})]^{1/2}$.

OT:PSS annealing and Al deposition) and cell characterization were performed in air. Power conversion efficiency was determined from *J*–*V* curve measurement (using a Keithley 2400 sourcemeter) under white light illumination (at 100 mW cm^{-2}). For white light efficiency measurements, Oriel 66002 solar light simulator with AM1.5 filter was used. Light intensity was measured by a Molectron Power Max 500D laser power meter. For the measurement of the external quantum efficiency, different wavelengths were selected with a Oriel Cornerstone 74000 monochromator, while the photocurrent was measured with a Keithley 2400 sourcemeter. The light intensity was measured with a Newport 1830-C optical power meter equipped with a 818-UV detector probe.

5. X-ray crystallography

Diffraction data were collected at 293 K using graphite-monochromated Mo Kα radiation (λ = 0.71073 Å) on a Bruker Axs SMART 1000 CCD diffractometer. The collected frames were processed with the software SAINT+ [83] and an absorption correction (SADABS) [84] was applied to the collected reflections. The structure was solved by the Direct methods (SHELXTL) [85] in conjunction with standard difference Fourier techniques and subsequently refined by full-matrix least-squares analyses on F^2. Hydrogen atoms were generated in their idealized positions and all non-hydrogen atoms were refined anisotropically. The relevant crystal data are given in Table 4.

Acknowledgements

This work was supported by a CERG Grant from the Hong Kong Research Grants Council (HKBU202607) and a Faculty Research Grant from the Hong Kong Baptist University (FRG/06-07/II-63). Financial support from the Strategic Research Theme, University Development Fund, and Seed Funding Grant and Outstanding Young Researcher Award (administrated by The University of Hong Kong) is also acknowledged.

Appendix A. Supplementary material

CCDC 694929 and 694930 contain the supplementary crystallographic data for this paper. These data can be obtained free of charge from The Cambridge Crystallographic Data Centre via www.ccdc.cam.ac.uk/data_request/cif. Supplementary data associated with this article can be found, in the online version, at doi:10.1016/j.jorganchem.2008.08.025.

References

[1] T.A. Skotheim, R.L. Elesenbaumer, J.R. Reynolds (Eds.), Handbook of Conducting Polymers, second ed., Marcel Dekker, New York, 1998.
[2] H.S. Nalwa (Ed.), Handbook of Organic Conductive Molecules and Polymers, vols. 1–4, Wiley, Chichester, UK, 1997.
[3] C.K. Chiang, Y.W. Park, A.J. Heeger, H. Shirakawa, E.J. Louis, A.G. McDiarmid, Phys. Rev. Lett. 39 (1977) 1098.
[4] A.O. Patil, A.J. Heeger, F. Wudl, Chem. Rev. 88 (1988) 183.
[5] Q. Pei, G. Yu, C. Zhang, Y. Yang, A.J. Heeger, Science 269 (1995) 1086.
[6] M. Herold, J. Gmeiner, M. Schworer, Acta Polym. 451 (1994) 392.
[7] D. Braun, A.J. Heeger, Appl. Phys. Lett. 58 (1991) 1982.
[8] P.L. Burns, A.B. Holmes, A. Kraft, D.D.C. Bradley, A.R. Brown, R.H. Friend, R.W. Gywer, Nature (London) 356 (1992) 47.
[9] A.J. Heeger, Solid State Commun. 49 (1998) 319.
[10] J.S. Wilson, A.S. Dhoot, A.J.A.B. Seeley, M.S. Khan, A. Kohler, R.H. Friend, Nature (London) 413 (2001) 828.
[11] N.S. Sariciftci, L. Smilowitz, A.J. Heeger, F. Wudl, Science 258 (1992) 1474.
[12] C.J. Brabec, N.S. Sariciftci, J.C. Hummelem, Adv. Funct. Mater. 11 (2001) 15.
[13] D. Wohrle, D. Meissner, Adv. Mater. 3 (1991) 129.
[14] J.J.M. Hall, C.A. Walsh, N.C. Greenham, E.A. Marseglia, R.H. Friend, S.S. Morattii, A.B. Holmes, Nature (London) 376 (1995) 498.
[15] S. Gunes, H. Neugebauer, N.S. Sariciftci, Chem. Rev. 107 (2007) 1324.
[16] K.M. Coakley, M.D. McGehee, Chem. Mater. 16 (2004) 4533.
[17] G. Yu, J. Wang, J. McElvain, A.J. Heeger, Adv. Mater. 10 (1998) 1431.
[18] L. Smilowitz, N.S. Sariciftci, R. Wu, C. Gettinger, A.J. Heeger, F. Wudl, Phys. Rev. B 47 (1993) 13835.
[19] B.C. Thompson, J.M.J. Fréchet, Angew. Chem., Int. Ed. 47 (2008) 58.
[20] K. Faid, M. Leclerc, Chem. Commun. (1996) 2761.
[21] D.T. McQuade, A.E. Pullen, T.M. Swager, Chem. Rev. 100 (2000) 2537.
[22] N.C. Greenham, R.H. Friend, Solid State Phys. 49 (1995) 1.
[23] Z. Bao, J. Lovinger, A.J. Brown, J. Am. Chem. Soc. 120 (1998) 207.
[24] J.A. Turner, Science 285 (1999) 687.
[25] S.E. Shaheen, D.S. Ginley, G.E. Jabbour, MRS Bull. 30 (2005) 10.
[26] K.W.J. Barnham, M. Mazze, B. Clive, Nature (London) 5 (2006) 161.
[27] W. Ma, C. Yang, X. Gong, K. Lee, A.J. Heeger, Adv. Funct. Mater. 15 (2005) 1617.
[28] G. Li, V. Shrotriya, J.S. Huang, Y. Yao, T. Moriarty, K. Emery, Y. Yang, Nat. Mater. 4 (2005) 864.
[29] J.Y. Kim, S.H. Kim, H.H. Lee, K. Lee, W. Ma, X. Gong, A.J. Heeger, Adv. Mater. 18 (2006) 572.
[30] J. Peet, J.Y. Kim, N.E. Coates, W.L. Ma, D. Moses, A.J. Heeger, G.C. Bazan, Nat. Mater. 6 (2007) 497.
[31] K. Kim, J. Liu, M.A.G. Namboothiry, D.L. Carroll, Appl. Phys. Lett. 90 (2007) 163511.
[32] J.Y. Kim, K. Lee, N.E. Coates, D. Moses, T.-Q. Nguyen, M. Dante, A.J. Heeger, Science 317 (2007) 222.
[33] M. Campoy-Quiles, T. Ferenczi, T. Agostinelli, P.G. Etchegoin, Y. Kim, T.D. Anthopoulos, P.N. Stavrinou, D.D.C. Bradley, J. Nelson, Nat. Mater. 7 (2008) 158.
[34] B. Minnaert, M. Burgelman, Prog. Photovolt: Res. Appl. 15 (2007) 741.
[35] S.A. Jenekhe, S. Yi, Appl. Phys. Lett. 77 (2000) 2635.
[36] C.J. Brabec, C. Winder, N.S. Sariciftci, J.C. Hummelen, A. Van Hal, P.A. Dhanabalan, R.A.J. Janssen, Adv. Funct. Mater. 12 (2002) 709.
[37] C. Winder, N.S. Sariciftci, J. Mater. Chem. 14 (2004) 1077.
[38] J. Roncali, Chem. Rev. 97 (1997) 173.
[39] J. Roncali, Macromol. Rapid Commun. 28 (2007) 1761.
[40] Q. Zhou, Q. Hou, L. Zheng, X. Deng, G. Yu, Y. Cao, Appl. Phys. Lett. 84 (2004) 1653.
[41] M. Svensson, F.Z. Veestra, C.S. Verhees, J.H. Weljon, J.C. Hummelen, J.M. Kroon, O. Inganäs, M.R. Andersson, Adv. Mater. 15 (2003) 988.
[42] W.-Y. Wong, K.-H. Choi, G.-L. Lu, J.-X. Shi, Macromol. Rapid Commun. 22 (2001) 461.
[43] S. Akoudad, J. Roncali, Chem. Commun. (1998) 2081.
[44] J.-M. Raimundo, P. Blanchard, H. Brisset, S. Akoudad, J. Roncali, Chem. Commun. (2000) 939.
[45] I.F. Perepichka, D.F. Perepichka, H. Meng, F. Wudl, Adv. Mater. 17 (2005) 2281.
[46] R.D. McCullough, Adv. Mater. 17 (2005) 2281.
[47] D. Fichou (Ed.), Handbook of Oligo- and Polythiophenes, Wiley-VCH, New York, 1999.
[48] T.-L. Stott, M.O. Wolf, Coord. Chem. Rev. 246 (2003) 89.
[49] Y. Xia, J. Luo, X. Deng, X. Li, D. Li, X. Zhu, W. Yang, Y. Cao, Macromol. Chem. Phys. 207 (2006) 511.
[50] F. Zhang, W. Mammo, L.M. Andersson, S. Admassie, M.R. Andersson, O. Inganäs, Adv. Mater. 18 (2006) 2169.

[51] F. Zhang, E. Perzon, X. Wang, W. Mammo, M.R. Andersson, O. Inganás, Adv. Funct. Mater. 15 (2005) 745.
[52] R.S. Ashraf, M. Shahid, E. Klemm, M. Al-Ibrahim, S. Sensfuss, Macromol. Rapid Commun. 27 (2006) 1454.
[53] J. Roncali, P. Blanchard, P. Frère, J. Mater. Chem. 15 (2005) 1589.
[54] P.D. Harvey, D. Fortin, Coord. Chem. Rev. 171 (1998) 351.
[55] W.-K. Chan, C.S. Hui, K.Y.K. Man, K.W. Cheng, H.L. Wong, N. Zhu, A.B. Djurišić, Coord. Chem. Rev. 249 (2005) 1351.
[56] W.-Y. Wong, Macromol. Chem. Phys. 209 (2008) 14.
[57] F. Guo, Y.G. Kim, J.R. Reynolds, K.S. Schanze, Chem. Commun. (2006) 1887.
[58] A. Köhler, H.F. Wittman, R.H. Friend, M.S. Khan, J. Lewis Synth. Met. 77 (1996) 147.
[59] N. Chawdhury, A. Köhler, R.H. Friend, W.Y. Wong, J. Lewis, M. Younus, P.R. Raithby, T.C. Corcoran, M.R.A. Al-Mandhary, M.S. Khan, J. Chem. Phys. 110 (1999) 4963.
[60] W.-Y. Wong, X.-Z. Wang, Z. He, A.B. Djurišić, C.-T. Yip, K.-Y. Cheung, H. Wang, C.S.-K. Mak, W.-K. Chan, Nat. Mater. 6 (2007) 521.
[61] W.-Y. Wong, X.-Z. Wang, Z. He, K.-K. Chan, A.B. Djurišić, K.-Y. Cheung, C.-T. Yip, A.M.-C. Ng, Y.-Y. Xi, C.S.-K. Mak, W.-K. Chan, J. Am. Chem. Soc. 129 (2007) 14372.
[62] M. Younus, A. Köhler, S. Cron, N. Chawdhury, M.R.A. Al-Mandhary, M.S. Khan, J. Lewis, N.J. Long, R.H. Friend, P.R. Raithby, Angew. Chem., Int. Ed. 37 (1998) 3036.
[63] X.-Z. Wang, W.-Y. Wong, K.-Y. Cheung, M.-K. Fung, A.B. Djurišić, W.-K. Chan, Dalton Trans., in press.
[64] N.J. Long, C.K. Williams, Angew. Chem., Int. Ed. 42 (2003) 2586.
[65] W.-Y. Wong, C.-L. Ho, Coord. Chem. Rev. 250 (2006) 2627.
[66] W.-Y. Wong, J. Inorg. Organomet. Polym. Mater. 15 (2005) 197.
[67] W.-Y. Wong, Dalton Trans. (2007) 4495.
[68] C. Kitamura, S. Tanaka, Y. Yamashita, Chem. Mater. 8 (1996) 570.
[69] S. Takahashi, Y. Kuroyama, K. Sonogashira, N. Hagihara, Synthesis (1980) 627.
[70] U.H.F. Bunz, Chem. Rev. 100 (2000) 1605. and references cited therein.
[71] E.E. Havinga, W. ten Hoeve, H. Wynberg, Synth. Met. 55–57 (1993) 299.
[72] J.L. Bredas, Synth. Met. 17 (1987) 115.
[73] M.S. Khan, M.K. Al-Suti, M.R.A. Al-Mandhary, B. Ahrens, J.K. Bjernemose, M.F. Mahon, L. Male, P.R. Raithby, R.H. Friend, A. Köhler, J.S. Wilson, Dalton Trans. (2003) 65.
[74] J.S. Wilson, N. Chawdhury, M.R.A. Al-Mandhary, M. Younus, M.S. Khan, P.R. Raithby, A. Köhler, R.H. Friend, J. Am. Chem. Soc. 123 (2001) 9412.
[75] J. Hou, Z. Tan, Y. Yan, Y. He, C. Yang, Y. Li, J. Am. Chem. Soc. 128 (2006) 4911.
[76] X. Wang, E. Perzon, F. Oswald, F. Langa, S. Admassie, M.R. Andersson, O. Inganäs, Adv. Funct. Mater. 15 (2005) 1665.
[77] L.J.A. Koster, V.D. Mihailetchi, R. Ramaker, P.W.M. Blom, Appl. Phys. Lett. 86 (2005) 123509.
[78] J. Xue, S. Uchida, B.P. Rand, S.R. Forrest, Appl. Phys. Lett. 84 (2004) 3013.
[79] I. Riedel, J. Parisi, V. Dyakonov, L. Lutsen, D. Vanderzande, J.C. Hummelen, Adv. Funct. Mater. 14 (2004) 38.
[80] J. Chatt, R.G. Hayter, J. Chem. Soc. Dalton Trans. (1961) 896.
[81] J. Chatt, B.L. Shaw, J. Chem. Soc. (1960) 4020.
[82] C.A. Parker, W.T. Rees, Analyst 85 (1960) 587.
[83] SAINT+, ver. 6.02a, Bruker, Analytical X-ray System, Inc., Madison, WI, 1998.
[84] G.M. Sheldrick, SADABS, Empirical Absorption Correction Program, University of Göttingen, Germany, 1997.
[85] G.M. Sheldrick, SHELXTL™, Reference Manual, ver. 5.1, Madison, WI, 1997.